

# Crystallization Kinetics of Bioactive Glasses in the ZnO–Na<sub>2</sub>O–CaO–SiO<sub>2</sub> System

Gianluca Malavasi,<sup>†</sup> Gigliola Lusvardi,<sup>†</sup> Alfonso Pedone,<sup>†</sup> Maria Cristina Menziani,<sup>†</sup>  
Monica Dappiaggi,<sup>‡</sup> Alessandro Gualtieri,<sup>§</sup> and Ledi Menabue<sup>\*,†</sup>

Department of Chemistry and SCS Centre, University of Modena and Reggio Emilia, Via Campi 183, 41100 Modena, Italy, Department of Earth Science, University of Milano, Via Mangiagalli 34, 20133 Milano, Italy, and Department of Earth Science, University of Modena and Reggio Emilia, Via Sant'Eufemia 19, 41100 Modena, Italy

Received: February 23, 2007; In Final Form: May 25, 2007

The crystallization kinetics of Na<sub>2</sub>O·CaO·2SiO<sub>2</sub> ( $x = 0$ ) and 0.68ZnO·Na<sub>2</sub>O·CaO·2SiO<sub>2</sub> ( $x = 0.68$ , where  $x$  is the ZnO stoichiometric coefficient in the glass formula) bioactive glasses have been studied using both nonisothermal and isothermal methods. The results obtained from isothermal XRPD analyses have showed that the first glass crystallizes into the isochemical Na<sub>2</sub>CaSi<sub>2</sub>O<sub>6</sub> phase, whereas the Na<sub>2</sub>ZnSiO<sub>4</sub> crystalline phase is obtained from the Zn-rich glass, in addition to Na<sub>2</sub>CaSi<sub>2</sub>O<sub>6</sub>. The activation energy ( $E_a$ ) for the crystallization of the Na<sub>2</sub>O·CaO·2SiO<sub>2</sub> glass is  $193 \pm 10$  and  $203 \pm 5$  kJ/mol from the isothermal in situ XRPD and nonisothermal DSC experiments, respectively. The Avrami exponent  $n$  determined from the isothermal method is 1 at low temperature (530 °C), and its value increases linearly with temperature increase up to 2 at 607 °C. For the crystallization of Na<sub>2</sub>CaSi<sub>2</sub>O<sub>6</sub> from the Zn-containing glass, higher values of both the crystallization temperature (667 and 661 °C) and  $E_a$  ( $223 \pm 10$  and  $211 \pm 5$  kJ/mol) have been found from the isothermal and nonisothermal methods, respectively. The Na<sub>2</sub>ZnSiO<sub>4</sub> crystalline phase crystallizes at lower temperature with respect to Na<sub>2</sub>CaSi<sub>2</sub>O<sub>6</sub>, and the  $E_a$  value is  $266 \pm 20$  and  $245 \pm 15$  kJ/mol from the isothermal and nonisothermal methods, respectively. The results of this work show that the addition of Zn favors the crystallization from the glass at lower temperature with respect to the Zn-free glass. In fact, it causes an increase of  $E_a$  for the Na diffusion process, determined using MD simulations, and consequently an overall increase of  $E_a$  for the crystallization process of Na<sub>2</sub>CaSi<sub>2</sub>O<sub>6</sub>. Our results show good agreement between the  $E_a$  and  $n$  values obtained with the two different methods and confirm the reliability of the nonisothermal method applied to kinetic crystallization of glassy systems. This study allows the determination of the temperature stability field of the crystalline phases with the view of creating a different glass ceramic useful in the field of bioactive materials.

## 1. Introduction

Crystallization kinetics is a fundamental tool of analysis for the development and optimization of advanced glass ceramics for novel applications. In the field of bioactive materials, modification of the crystallization paths and kinetics is particularly interesting since it can be exploited to tailor a great range of properties and to favor the linking speed to the tissues.<sup>1</sup>

For example, the heat treating of bioactive glass 45S5 to induce 8–100% crystallization (crystalline phase obtained, Na<sub>2</sub>Ca<sub>2</sub>Si<sub>3</sub>O<sub>9</sub>) slightly reduces the rate of surface hydroxyapatite formation with respect to amorphous bioactive glass 45S5.<sup>2</sup> The dissolution rate and, consequently, in vitro bioactive response of 45S5 glass ceramic seem to depend on the type and quantity of crystalline phase developed during the thermal treatment.<sup>3</sup> The presence of bioactive glass 45S5 dissolution products has been shown to influence gene transcription in osteoblasts in vitro.<sup>4</sup> It has been recently demonstrated that Zn, an essential trace element, manifests stimulatory effects on bone formation in vitro and in vivo.<sup>5</sup> In fact, the slow release of Zn incorporated

into an implant material promotes bone formation around the implant and accelerates recovery of the patient.<sup>5</sup> Moreover, it is well-known that the addition of Zn to silicate glasses can promote the crystallization of crystal phases that increases the bending strength of glass ceramics.<sup>6</sup>

In view of the effect of glass crystallization on the glass bioactivity and cellular reactions, this paper presents the study of the crystallization process of Na<sub>2</sub>O·CaO·2SiO<sub>2</sub> ( $x = 0$ ) and its Zn derivative of composition 0.68ZnO·Na<sub>2</sub>O·CaO·2SiO<sub>2</sub> ( $x = 0.68$ , where  $x$  is the ZnO stoichiometric coefficient in the glass formula) using the Avrami<sup>7</sup> nucleation–growth model.

This model, originally developed to describe isothermal crystallization, has been extended to the description of nonisothermal data only in a limited number of cases.<sup>7</sup> Since generally an isothermal experiment is more time demanding than a nonisothermal one, the comparison between the parameters derived with both experiments could confirm the reliability of the nonisothermal method for the kinetics parameter calculations of silicate glasses.

The isothermal crystallization has been analyzed by X-ray powder diffraction (XRPD), while differential scanning calorimetry (DSC) analysis has been performed for nonisothermal crystallization.

For a deeper understanding of the crystallization processes, transmission electron microscopy (TEM) has been also used

\* Corresponding author. Telephone: +390592055042. Fax: +390593-73543. E-mail: menabue.ledi@unimore.it.

<sup>†</sup> Department of Chemistry and SCS Centre, University of Modena and Reggio Emilia.

<sup>‡</sup> University of Milano.

<sup>§</sup> Department of Earth Science, University of Modena and Reggio Emilia.

for the determination of the crystal morphology, and classical molecular dynamics (MD) simulations<sup>8,9</sup> have been performed to determine the coefficients and activation energies of diffusion processes of the glass constituents.

In view of these considerations, the knowledge of the crystallization kinetics process of soda lime silicate and Zn-containing glasses may be used to obtain glass ceramics with the desired dissolution rates and able to favor the gene expression of osteoblasts in vivo.

## 2. Experimental Methods

The glasses  $\text{Na}_2\text{O}\cdot\text{CaO}\cdot 2\text{SiO}_2$  ( $x = 0$ ) and  $0.68\text{ZnO}\cdot\text{Na}_2\text{O}\cdot\text{CaO}\cdot 2\text{SiO}_2$  ( $x = 0.68$ ) were prepared as described by Lusvardi et al.,<sup>8</sup> and their compositions in mole percent (mol %) are as follows: for  $x = 0$ , 50%  $\text{SiO}_2$ , 25%  $\text{Na}_2\text{O}$ , 25%  $\text{CaO}$ ; and for  $x = 0.68$ , 42.8%  $\text{SiO}_2$ , 21.4%  $\text{Na}_2\text{O}$ , 21.4%  $\text{CaO}$ , 14.4%  $\text{ZnO}$ . The glass named  $x = 0$  corresponds to the bioactive 50S glass prepared by Kokubo and co-workers.<sup>10</sup>

The melts were poured onto stainless steel plates, ball milled in agate mill jars, and sieved to produce a particle size range of  $90 < \phi < 106 \mu\text{m}$ . The obtained powders were used for XRPD, DSC, and TEM analyses. This particle dimension assures no preference toward surface nucleation.<sup>11</sup>

**XRPD Analysis.** In situ XRPD analyses in isothermal mode were utilized to determine the kinetic parameters.<sup>12</sup> Preliminary XRPD analyses ( $10\text{--}70^\circ 2\theta$  range, counting time 0.5 s for each  $0.03^\circ 2\theta$  step) were performed to identify the crystalline phases obtained by crystallization of  $x = 0$  and  $x = 0.68$  glasses after a thermal treatment around the crystallization temperature, as reported in our previous work.<sup>8</sup> The crystalline phase obtained by crystallization of  $x = 0$  glass was  $\text{Na}_2\text{CaSi}_2\text{O}_6$  (Joint Committee on Powder Diffraction Standards, JCPDS, 77-2189); and in the  $x = 0.68$  glass, the most important crystalline phases observed were  $\text{Na}_2\text{CaSi}_2\text{O}_6$  and  $\text{Na}_2\text{ZnSiO}_4$  (JPCDS 37-0407), as reported in ref 8. The XRPD analyses were also used for (i) the evaluation of the rate for subsequent experiments and (ii) the determination of the angular regions of the powder pattern to be collected in the isothermal runs.

In situ XRPD analyses were performed using a PANalytical X'Pert Pro Bragg–Brentano diffractometer with  $\text{Cu K}\alpha$  radiation. The time-resolved isothermal runs for the kinetic analyses of the  $x = 0$  glass were performed in the angular range  $32\text{--}35^\circ 2\theta$  (counting time was 1 s for each  $0.03^\circ 2\theta$  step) in order to follow the temperature evolution of the main peak ( $d_{220} = 2.6250 \text{ \AA}$  ( $34.129^\circ 2\theta$ ),  $I/I_0 = 100\%$ ) of  $\text{Na}_2\text{CaSi}_2\text{O}_6$  during the crystallization process. Isothermal runs were performed at 530, 542, 557, 572, 587, 600, and  $607^\circ \text{C}$  around the onset temperature for the crystallization process. The total length of each isothermal experiment varied from 24 h at  $530^\circ \text{C}$  to 2 h at  $607^\circ \text{C}$ . For an accurate determination of kinetic parameters, another isothermal run at  $570^\circ \text{C}$  (close to the mean value of range temperature) was performed to verify the agreement between the results.

The time-resolved isothermal runs for the kinetic analysis of  $x = 0.68$  glass were performed in the angular range  $46\text{--}50^\circ 2\theta$  to follow the temperature evolution of one peak of  $\text{Na}_2\text{CaSi}_2\text{O}_6$  ( $d_{404} = 1.8713 \text{ \AA}$  ( $48.614^\circ 2\theta$ ),  $I/I_0 = 58\%$ ) and one peak of  $\text{Na}_2\text{ZnSiO}_4$  ( $d_{402} = 1.8530 \text{ \AA}$  ( $49.124^\circ 2\theta$ ),  $I/I_0 = 11\%$ ). Data were collected under the same conditions adopted for the  $x = 0$  glass. Isothermal runs were performed at 563, 573, 580, 590, 598, 600, and  $608^\circ \text{C}$  around the onset temperature for the crystallization process. The total length of each isothermal experiment varied from 20 h at  $563^\circ \text{C}$  to 2 h at  $608^\circ \text{C}$ .

Each isothermal run involves a rapid temperature ramp ( $30^\circ \text{C}/\text{min}$ ) to reach the desired isothermal temperature. The experimental time was sufficient to reach a steady state of the crystallization process. The evolution of the crystallization process as a function of time has been followed by measuring the integrated intensity of the peak ( $d_{404}$  for  $\text{Na}_2\text{CaSi}_2\text{O}_6$  and  $d_{402}$  for  $\text{Na}_2\text{ZnSiO}_4$ ) chosen by the routine X'Pert HighScore (version 1.0a by PANalytical, B.V., Almelo, Netherlands). The normalized integrated intensities were then transformed into phase volume fraction crystallized  $\alpha$  ( $\alpha =$  the normalized volume fraction of crystallized material from glass relative to the final peak area).<sup>12</sup>

Several analytical methods, derived from the Avrami model,<sup>7</sup> have been suggested to investigate the nucleation and growth mechanism using nonisothermal DSC data.<sup>13</sup> The details of the methods used in this paper are briefly reported.

**Isothermal Method.** The kinetics of isothermal glass crystallization are generally studied using methods based on the Avrami equation:<sup>14,7</sup>

$$\alpha = 1 - \exp[-(kt)^n] \quad (1)$$

where  $\alpha$  is the volume fraction isothermally crystallized at the time  $t$ ,  $k$  is the rate constant, and  $n$  is the Avrami exponent. The Avrami exponent is used to determine the crystal growth morphology and the nature of the crystallization process, which can be controlled mainly by diffusion or phase boundary. The data analysis was performed following the standard procedure after Henchcock and Sharp<sup>15</sup> and includes the plot of the quantity  $\ln(-\ln(1 - \alpha))$  versus  $\ln(t)$ . The slope of the regression line fitted through the points at each temperature is characteristic of the kinetic expression and is commonly defined as  $n$ .<sup>16</sup> The plots of  $(-\ln(1 - \alpha))^{1/n}$  versus  $t$  allow the calculation of the rate constants  $k$  (slope of the regression line) for each isothermal run. The values of the obtained  $k$  are then used in the plot of  $\ln(k)$  versus  $1/T$ , the logarithmic form of the Arrhenius equation:

$$k = A \exp(-E_a/RT) \quad (2)$$

where  $A$  is the frequency factor,  $E_a$  is the apparent activation energy of the process,  $R$  is the gas constant, and  $T$  is the absolute temperature.

**Nonisothermal Method.** (i) Assuming a constant heating ratio  $\beta$ , the Avrami exponent  $n$  at a fixed temperature  $T$  is computed by using Ozawa's method:<sup>17</sup>

$$\ln(-\ln(1 - \alpha)) = -n \ln \beta + \text{const} \quad (3)$$

where  $\alpha$  is the volume fraction of crystallites,  $\beta$  is the heating rate, and  $n$  is the Avrami exponent. The slope of the plot of  $\ln(-\ln(1 - \alpha))$  versus  $\ln \beta$  is  $-n$ .

(ii)  $E_a$  can be evaluated by a modification<sup>18</sup> of the equation originally developed by Kissinger:<sup>19</sup>

$$\ln(T_p^2/\beta^n) = mE_a/RT_p + \text{const} \quad (4)$$

where  $T_p$  is the temperature corresponding to the maximum of the exothermic peak,  $E_a$  is the apparent activation energy (including the contribution from both nucleation and crystal growth), and  $m$  is the crystallization mechanism parameter. For three-dimensional (spherical) growth,  $m = 3$ , for two-dimensional (disklike growth)  $m = 2$ , and for surface or one-dimensional (rodlike growth)  $m = 1$ .<sup>20,21</sup> The slope of the plot of  $\ln(T_p^2/\beta^n)$  versus  $1/T_p$  is equal to the term  $mE_a/R$ .

The applicability of the Avrami model to the nonisothermal crystallization of the glasses studied in this paper was confirmed by the DSC exothermic peaks which show a fractional conver-

sion,  $\alpha$ , between 0.60 and 0.64 at the peak temperature,  $T_p$ , in the range of the investigated heating rates,  $\beta$ .<sup>22</sup>

The DSC analyses were used to determine the kinetic parameters using the nonisothermal method. DSC analyses were performed up to 1000 °C using 30 mg of powder glass with the following heating rates,  $\beta$ : 5, 10, 15, and 20 °C/min. The accuracy in the determination of the maximum position is due primarily to the accuracy of the DSC measurements, which is  $\pm 1$  °C. In fact, the difference between two replication measurements is less than 1 °C. The DSC equipment was calibrated periodically using CuSO<sub>4</sub>·5H<sub>2</sub>O and Na<sub>2</sub>SO<sub>4</sub>. The DSC instrument used was a LABSYS-Setaram, and the data were recorded and analyzed with a computer interfaced with the DSC equipment. Samples used for DSC were as-quenched glass, and no pre-nucleation treatment was induced. The peak crystallization temperature,  $T_p$ , was determined from the maximum position of the exothermic peak present in the DSC plot for the  $x = 0$  glass, while for the  $x = 0.68$  glass three exothermic peaks due to different crystallization processes were found. As reported in a previous work<sup>8</sup> the third peak (around 660 °C) was attributed to the crystallization of Na<sub>2</sub>CaSi<sub>2</sub>O<sub>6</sub>. Further XRPD analyses, performed in the present work around the temperature corresponding to the second exothermic peak of the DSC plot (range 600–620 °C), showed that the main crystalline phase was Na<sub>2</sub>ZnSiO<sub>4</sub>; therefore, the most intense peak at 613 °C was attributed to Na<sub>2</sub>ZnSiO<sub>4</sub>.<sup>8</sup>

The volume fraction  $\alpha$  was determined from the DSC plot for the nonisothermal method. At a fixed temperature  $T$ , the value of  $\alpha$  for each  $\beta$  value is given as  $\alpha = A_T/A$ , where  $A$  is the total area of the exothermic peak and corresponds to the complete crystallization process and  $A_T$  is the partial area of the exothermic peak from the beginning temperature of the peak and temperature  $T$ .

**TEM Analysis.** The morphology of crystal phases obtained after 1 h of thermal treatment was determined using a TEM instrument Jeol JEM 2010 equipped with an energy dispersive spectrometer (EDS). These measurements were performed on glass powders with the same sizes used for the thermal treatment at temperatures of 600 °C for  $x = 0$  and 660 °C for  $x = 0.68$ .

**MD Simulations: Determination of Transport Properties.** The glass structures of  $x = 0$  and  $x = 0.68$  were modeled by means of NVT molecular dynamics (MD) simulations. For each composition, three simulations were performed with  $\sim 1200$  atoms placed randomly in a cubic box to generate the initial configurations. Atomic compositions and size length of the simulation boxes are reported in ref 8, together with the glass densities at room temperature.

The DL\_POLY<sup>23</sup> package and the force field developed by Pedone et al.<sup>24</sup> were used in this work for MD simulations. The force field is based on a rigid ionic model, with partial charges to handle the partial covalency of silicate systems.

Transport properties of the systems were determined at eight different temperatures (700, 800, 850, 900, 1000, 1300, 1600, and 2000 K) below the glass transition temperature of the glass in the framework of the interatomic potentials used. The difference between the experimental glass transition temperature (510 °C for  $x = 0$  and 494 °C for  $x = 0.68$ , ref 8) and the computational one is mainly due to the MD simulation procedure and force field used. Two practical aspects of MD simulations require emphasis. First, the limited number of atoms included in the simulation box is inevitably a compromise between the available computer resources (CPU time, primarily) and the desire to have as many atoms as possible in the model. Because this number is always small compared to Avogadro's number, periodic boundary conditions are used to create an infinite solid, that is, one with no external surfaces. This has thermodynamic ramifications, because the lack of surfaces makes the system

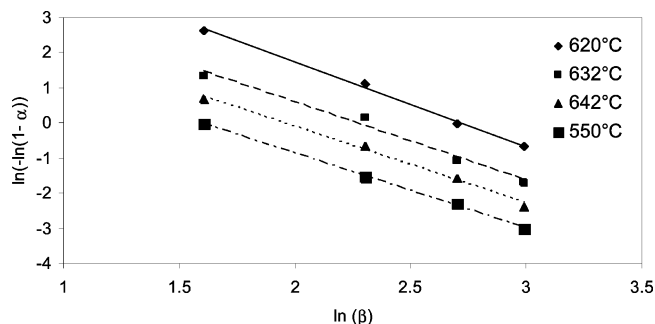


**Figure 1.** Plot of  $\ln(-\ln(1 - \alpha))$  vs  $\ln(\beta)$  at 620, 632, 642 and 650 °C for  $x = 0$  glass.

more susceptible to superheating and supercooling. This will impact the procedure used to form the glass in the computer. In addition, the boundary conditions require structural coherence across the faces of the simulation box. Both of these effects will result in the simulated glass structure having a higher effective internal temperature than the target temperature. However, fictive temperatures, which are usually derived from considerations of the nominal cooling rate, will severely overestimate the actual effective internal temperature.<sup>25</sup>

For each system the configuration at 300 K was reheated using a Berendsen barostat<sup>26</sup> with frictional constants set to 0.4 ps. At each temperature the systems were relaxed for 40 ps followed by 10 ns of data production, during which configurations were saved at intervals of 1 ps and used subsequently to calculate dynamic properties.

The mean square displacement (msd), which is a measure of the average distance a molecule travels, is defined according to

$$\text{msd}_j(t) = \frac{1}{N_j} \sum_{i=1}^{N_j} \langle \Delta \mathbf{r}_i(t)^2 \rangle = \frac{1}{N_j} \sum_{i=1}^{N_j} \langle (\mathbf{r}_i(t) - \mathbf{r}_i(t_0))^2 \rangle \quad (5)$$

where  $\mathbf{r}_i(t) - \mathbf{r}_i(t_0)$  is the (vector) distance traveled by atom  $i$  over some time intervals of length  $t$ , and the squared magnitude of this vector is averaged (as indicated by the brackets) over many such time intervals. To improve statistical accuracy, this quantity is also averaged over all atoms of  $j$ th species in the system.

The limiting slope of  $\text{msd}(t)$ , considered for time intervals sufficiently long for it to be in the linear regime (from 2 to 9 ns), is related to the self-diffusion constant  $D$  by the Einstein relation:

$$\lim_{t \rightarrow \infty} \frac{d}{dt} \langle \Delta \mathbf{r}_i(t)^2 \rangle = 2dD \quad (6)$$

where  $d$  is the dimension of the space ( $d = 3$  for three-dimensional diffusion).

### 3. Results

**Kinetic Analysis with Nonisothermal Method.**  $x = 0$  (S50) Glass. Figure 1 reports the plot of  $\ln(-\ln(1 - \alpha))$  vs  $\ln(\beta)$  at 620, 632, 642, and 650 °C. The negative slope of each plot is equal to the Avrami exponent  $n$ . The average Avrami exponent, determined by eq 3, is  $2.2 \pm 0.2$ . For each temperature a value of  $n$  close to 2 is found; therefore, only one mechanism is possible for the crystallization of Na<sub>2</sub>CaSi<sub>2</sub>O<sub>6</sub>. Figure 2 shows the Kissinger plot for the glass heated at a heating rate  $\beta$  in the range 5–20 °C/min. The least-squares fit yielded a value of  $mE_a = 406 \pm 10$  kJ/mol, determined by eq 4.

$x = 0.68$  Glass. The plot of  $\ln(-\ln(1 - \alpha))$  vs  $\ln(\beta)$  at different temperatures, relative to the DSC peaks attributed to

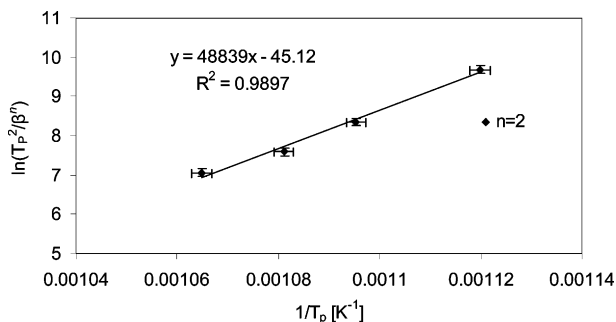


**Figure 2.** Plot of  $\ln(T_p^2/\beta^n)$  vs  $T_p^{-1}$  for  $x = 0$  glass.

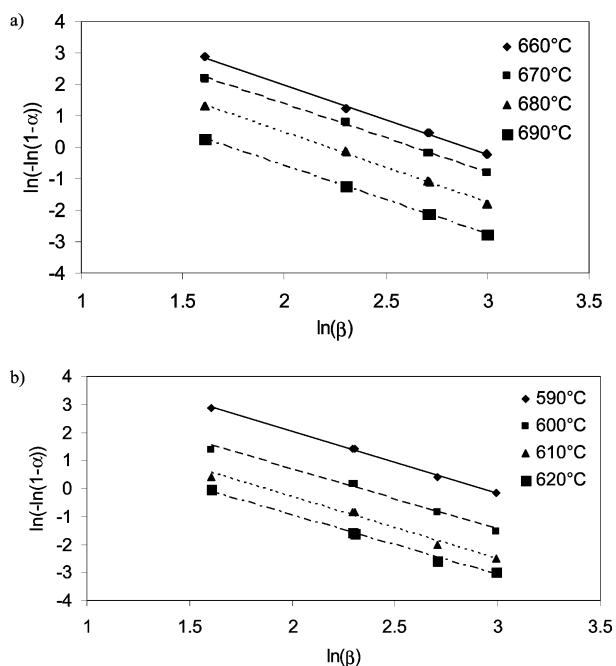


**Figure 3.** (a) Plot of  $\ln(-\ln(1 - \alpha))$  vs  $\ln(\beta)$  at 660, 670, 680, and 690 °C for the  $\text{Na}_2\text{CaSi}_2\text{O}_6$  crystallization process. (b) Plot of  $\ln(-\ln(1 - \alpha))$  vs  $\ln(\beta)$  at 590, 600, 610, and 620 °C for the  $\text{Na}_2\text{ZnSiO}_4$  crystallization process.

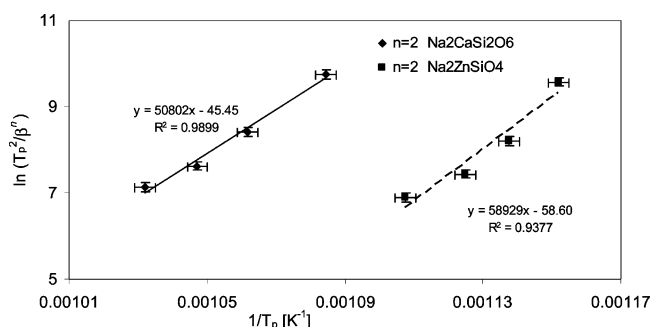


**Figure 4.** Plot of  $\ln(T_p^2/\beta^n)$  vs  $T_p^{-1}$  for the  $x = 0.68$  glass for the  $\text{Na}_2\text{CaSi}_2\text{O}_6$  crystallization process (♦) and the  $\text{Na}_2\text{ZnSiO}_4$  crystallization process (gray ■).

$\text{Na}_2\text{CaSi}_2\text{O}_6$  (DSC peak at  $\approx 660$  °C) and  $\text{Na}_2\text{ZnSiO}_4$  (DSC peak at  $\approx 613$  °C) crystallization, is reported in parts a and b, respectively, of Figure 3. The average  $n$  parameter reported in Figure 3a and Figure 3b is  $2.2 \pm 0.1$  and  $2.1 \pm 0.1$ , respectively. The  $n$  value close to 2 for each temperature suggests that only one crystallization mechanism occurs. The Kissinger plot using  $n = 2$  and heating rate in the range of 5–20 °C/min is shown in Figure 4. The least-squares fit yielded a value of  $mE_a = 422 \pm 10$  and  $490 \pm 30$  kJ/mol for  $\text{Na}_2\text{CaSi}_2\text{O}_6$  and  $\text{Na}_2\text{ZnSiO}_4$ , respectively.

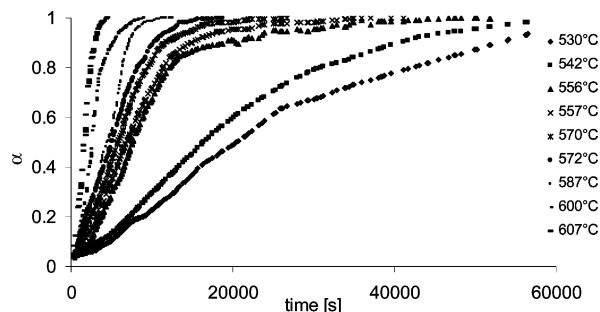


**Figure 5.** Crystallization fraction,  $\alpha$ , of  $x = 0$  glass as a function of isothermal time.

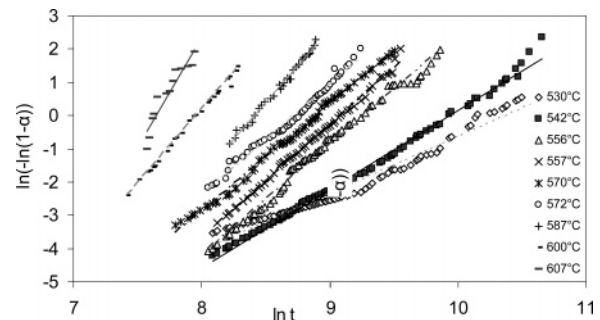


**Figure 6.** Plot of  $\ln(-\ln(1 - \alpha))$  versus  $\ln(t)$  for determining values of  $n$  of the as-quenched  $x = 0$  glass.

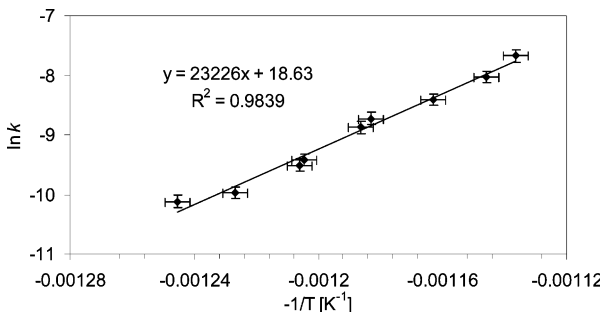


**Figure 7.** Arrhenius plot for calculation of  $E_a$  from the slope of the linear fit of  $\ln k$  vs  $-1/T$  for  $x = 0$  glass.

**Kinetic Analysis with Isothermal Method.  $x = 0$  Glass.** The  $\alpha$ -time plots are shown in Figure 5. As expected, a longer time is needed to complete crystallization at low temperatures compared to high temperatures. It is worth noting that high precision in the determination of  $\alpha$  is required,<sup>27</sup> since the values of the function  $\ln(-\ln(1 - \alpha))$  are strongly affected by slight differences in  $\alpha$  values for  $0 < \alpha < 0.1$ . At low  $\alpha$  values the exact measurement of small peak areas is very difficult and this may lead to incorrect slope values for the  $\ln(-\ln(1 - \alpha))$  versus  $\ln(t)$  plot. At the final stage of crystallization ( $\alpha > 0.9$ ), the saturation of nucleation sites and the mutual contacts of crystals also lead to deviation from linearity of the plot of  $\ln(-\ln(1 - \alpha))$  versus  $\ln(t)$ . To minimize such bias, the determination of  $n$  and  $k$  has been carried out in a limited range of  $\alpha$  values ( $0.1 < \alpha < 0.9$ ). The plots of  $\ln(-\ln(1 - \alpha))$  versus  $\ln(t)$  at different temperatures is shown in Figure 6.

The plots of  $\ln(1 - \alpha)$  versus  $t^n$  allow the calculation of the rate constant  $k$  for each isothermal run. Values of  $n$  and  $k$  have been determined by least-squares fits of the experimental data and summarized in Table 1. The value of  $n$  increases linearly with the temperature from 1.0 to 2.0. The values of  $k$  are used in the plot of  $\ln(k)$  vs  $-1/T$  (Figure 7). This plot yields the values of the apparent activation energy  $E_a = 193 \pm 10$  kJ/mol and the frequency factor  $A = (1.2 \pm 0.1) \times 10^8 \text{ s}^{-1}$ .

**TABLE 1: Values of Avrami Exponent ( $n$ ) and the Reaction Constant ( $k$ ) for the  $x = 0$  Glass for Different Isothermal Runs**

temp [°C] ± 1 °C	Avrami exponent $n \pm 0.1$	rate const $k$ [s <sup>-1</sup> ]
530	1.0	0.000 041 (4)
542	1.3	0.000 046 (5)
556	1.4	0.000 075 (5)
557	1.4	0.000 080 (7)
570	1.5	0.000 14 (1)
572	1.6	0.000 16 (1)
587	1.9	0.000 22 (2)
600	1.7	0.000 32 (2)
607	2.0	0.000 47 (3)

**TABLE 2: Values of the Avrami Exponent ( $n$ ) and the Reaction Constant ( $k$ ) for the Crystallization Process of Na<sub>2</sub>CaSi<sub>2</sub>O<sub>6</sub> and Na<sub>2</sub>ZnSiO<sub>4</sub> Phases in the  $x = 0.68$  Glass for Different Isothermal Runs**

crystal phase	temp [°C] ± 1 °C	Avrami exponent $n \pm 0.1$	rate const $k$ [s <sup>-1</sup> ]
Na <sub>2</sub> CaSi <sub>2</sub> O <sub>6</sub>	563	0.9	0.000 18 (2)
	573	1.0	0.000 25 (2)
	580	1.1	0.000 43 (3)
	590	1.4	0.000 50 (4)
	598	1.8	0.000 66 (4)
	600	1.9	0.000 72 (5)
	608	2.1	0.000 87 (7)
Na <sub>2</sub> ZnSiO <sub>4</sub>	563	0.9	0.000 063 (3)
	573	1.1	0.000 14 (1)
	580	1.2	0.000 16 (1)
	590	1.5	0.000 21 (1)
	598	2.0	0.000 33 (2)
	600	2.1	0.000 38 (3)
	608	2.2	0.000 43 (3)

$x = 0.68$  Glass. The procedure described above is used for this glass assuming two independent crystallization processes for Na<sub>2</sub>CaSi<sub>2</sub>O<sub>6</sub> and Na<sub>2</sub>ZnSiO<sub>4</sub>. The calculation of  $\alpha$  is performed considering the evolution of two not overlapping peaks belonging to Na<sub>2</sub>CaSi<sub>2</sub>O<sub>6</sub> and Na<sub>2</sub>ZnSiO<sub>4</sub>. Table 2 reports all the kinetic parameters determined for the crystallization process of the Na<sub>2</sub>CaSi<sub>2</sub>O<sub>6</sub> and Na<sub>2</sub>ZnSiO<sub>4</sub> crystalline phases. The  $n$  values increase from 0.9 to 2.1 for Na<sub>2</sub>CaSi<sub>2</sub>O<sub>6</sub> and from 0.9 to 2.2 for Na<sub>2</sub>ZnSiO<sub>4</sub> with temperature increase. These values are used in the plot of  $\ln(k)$  vs  $-1/T$  (Figure 8) to yield the values of  $E_a = 223 \pm 10$  kJ/mol and  $A = (1.6 \pm 0.2) \times 10^{10}$  s<sup>-1</sup> for the Na<sub>2</sub>CaSi<sub>2</sub>O<sub>6</sub> crystallization process (Figure 8) and  $E_a = 266 \pm 20$  kJ/mol and  $A = (3.1 \pm 0.3) \times 10^{12}$  s<sup>-1</sup> for the Na<sub>2</sub>ZnSiO<sub>4</sub> crystallization process.

**Morphological and Compositional Analysis.** The TEM micrograph reported in Figure 9a ( $x = 0$ ) shows a two-dimensional crystal morphology. In fact, a typical lamellar-shape characteristic of two-dimensional growth is observed. No

**TABLE 3: Diffusion Coefficients ( $D$ ) of Na, Ca, and Zn Ions at Different Temperatures for  $x = 0$  and  $x = 0.68$  Glasses Computed by MD Simulations**

glass	$T$ [K]	$D_{\text{Na}}$ [m <sup>2</sup> s <sup>-1</sup> ]	$D_{\text{Ca}}$ [m <sup>2</sup> s <sup>-1</sup> ]	$D_{\text{Zn}}$ [m <sup>2</sup> s <sup>-1</sup> ]
$x = 0$	700	$3.88 \times 10^{-11}$	$1.24 \times 10^{-13}$	
	800	$1.40 \times 10^{-10}$	$1.09 \times 10^{-12}$	
	850	$2.42 \times 10^{-10}$	$2.40 \times 10^{-12}$	
	900	$3.10 \times 10^{-10}$	$6.24 \times 10^{-12}$	
	1000	$5.44 \times 10^{-10}$	$2.35 \times 10^{-11}$	
	1300	$3.20 \times 10^{-9}$	$3.45 \times 10^{-10}$	
	1600	$7.52 \times 10^{-9}$	$2.55 \times 10^{-9}$	
	1800	$1.19 \times 10^{-8}$	$8.77 \times 10^{-9}$	
	2000	$2.15 \times 10^{-8}$	$1.87 \times 10^{-8}$	
	$x = 0.68$	700	$7.77 \times 10^{-12}$	$1.40 \times 10^{-13}$
800		$3.45 \times 10^{-11}$	$9.88 \times 10^{-13}$	$1.43 \times 10^{-13}$
850		$8.43 \times 10^{-11}$	$3.44 \times 10^{-12}$	$1.63 \times 10^{-12}$
900		$1.23 \times 10^{-10}$	$5.62 \times 10^{-12}$	$2.80 \times 10^{-12}$
1000		$4.21 \times 10^{-10}$	$1.99 \times 10^{-11}$	$7.37 \times 10^{-12}$
1300		$1.99 \times 10^{-9}$	$9.00 \times 10^{-10}$	$6.90 \times 10^{-10}$
1600		$4.80 \times 10^{-9}$	$3.15 \times 10^{-9}$	$2.79 \times 10^{-9}$
1800		$1.15 \times 10^{-8}$	$8.08 \times 10^{-9}$	$7.90 \times 10^{-9}$
2000		$2.05 \times 10^{-8}$	$1.89 \times 10^{-8}$	$1.83 \times 10^{-8}$

spherical crystals (three-dimensional growth) or rodlike crystals (one-dimensional growth) have been detected. The semiquantitative EDS analysis reveals that the particles are essentially composed of oxygen, silicon, sodium, and calcium. The analysis performed on  $x = 0.68$  powders shows crystals with a composition similar to the Zn-containing crystal phase Na<sub>2</sub>ZnSiO<sub>4</sub> and a crystal morphology which is likely the result of a two-dimensional crystal growth (Figure 9b).

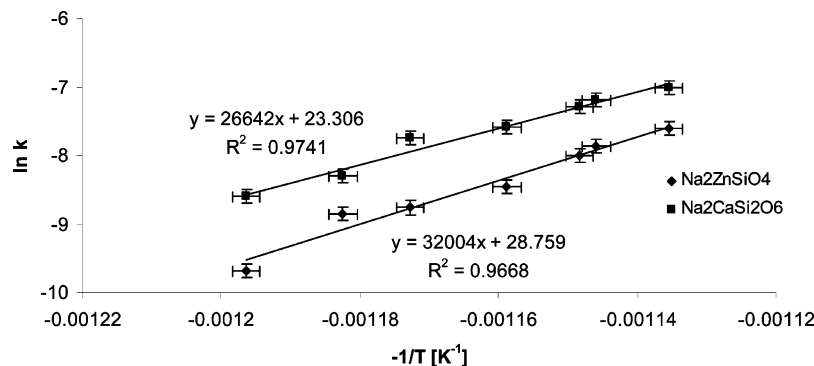
**Diffusion Properties.** The diffusion coefficients ( $D$ ) of Na, Ca, and Zn ions for the systems studied are listed in Table 3.

In the observed temperature range limit, sodium, calcium, and zinc diffusion can be described as an activated process:

$$D(T) = D_0 \exp(-E_a/RT) \quad (7)$$

with activation energy  $E_a$  and preexponential factor  $D_0$ , which is related to jump distance and frequency.

The  $\ln D$  vs  $-1/T$  plots for the  $x = 0$  and  $x = 0.68$  simulated glasses are shown in Figures 10 and 11, respectively. All the trends present a linear regression. The preexponential factor  $D_0$  and the activation energies ( $E_a$ ) obtained from the linear regression are listed in Table 4. The presence of Zn causes a decrement of the diffusion coefficients and an increment of  $E_a$  for sodium ions (from 55.0 for  $x = 0$  to 68.2 kJ/mol for  $x = 0.68$ ), whereas the data values of the calcium ions are unaffected. The  $E_a$  of the Zn ions (127.4 kJ/mol) is significantly higher with respect to those of calcium and sodium ions.

**Figure 8.** Arrhenius plot for calculation of  $E_a$  of Na<sub>2</sub>CaSi<sub>2</sub>O<sub>6</sub> (◆) and Na<sub>2</sub>ZnSiO<sub>4</sub> (■) from the slope of the linear fit of  $\ln k$  vs  $-1/T$  for  $x = 0.68$  glass.

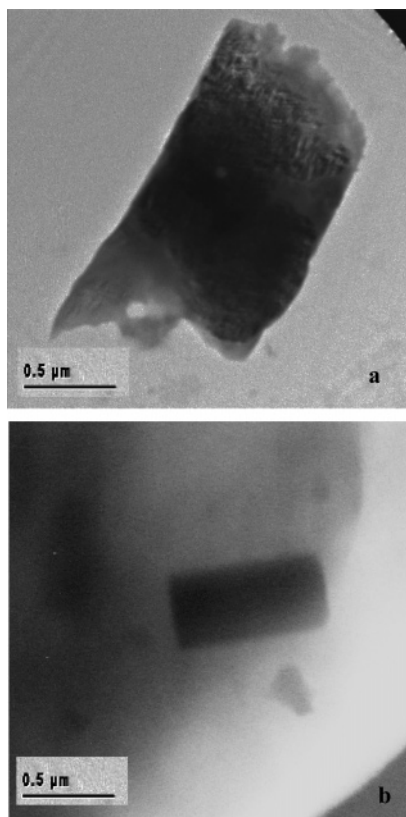


**Figure 9.** (a) TEM micrograph of a particle corresponding to  $\text{Na}_2\text{CaSi}_2\text{O}_6$  crystal phase in  $x = 0$  glass. (b) TEM micrograph of a particle corresponding to  $\text{Na}_2\text{ZnSiO}_4$  crystal phase in  $x = 0.68$  glass.

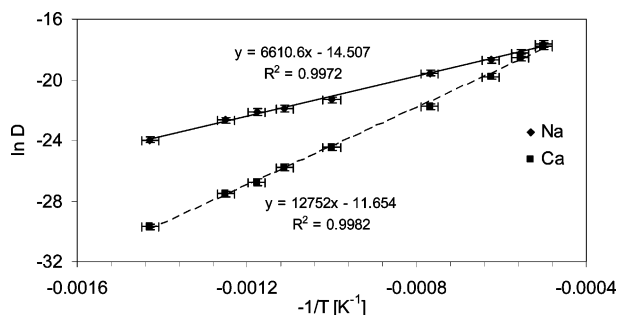


**Figure 10.** Arrhenius plots for calculation of  $E_a$  for diffusion process of (◆) Na and (■) Ca in  $x = 0$  glass.

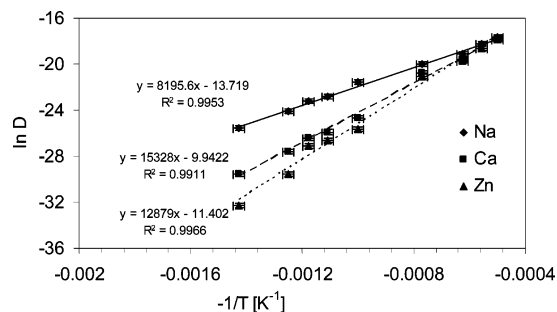


**Figure 11.** Arrhenius plots for calculation of  $E_a$  for diffusion process of (◆) Na, (■) Ca, and (▲) Zn in  $x = 0.68$  glass.

#### 4. Discussion

The Avrami exponent  $n$  can be utilized to determine the nature of the crystallization process mainly controlled by diffusion or phase boundary. The average particle size used in the litera-

**TABLE 4: Activation Energy ( $E_a$ ) and Preexponential Factor ( $D_0$ ) of Na, Ca, and Zn Ions for the Modeled Glasses**

glass	ion	$E_a$ [kJ/mol]	$D_0$ [ $\text{m}^2 \text{s}^{-1}$ ]
$x = 0$	Na	55.0	$5.01 \times 10^{-7}$
	Ca	106.8	$8.68 \times 10^{-6}$
$x = 0.68$	Na	68.2	$1.35 \times 10^{-5}$
	Ca	107.1	$1.12 \times 10^{-5}$
	Zn	127.4	$4.81 \times 10^{-5}$

ture<sup>18,28</sup> for the DSC nonisothermal method is smaller than 20  $\mu\text{m}$ ; the small particles assure the preference toward a phase boundary (surface) control and the determination of  $n$  shows univocally the type of growth. Under the conditions used in this work, the mechanism of growth is inferred by (i) the Avrami exponent  $n$ , (ii) the  $mE_a$  values found by the nonisothermal method, (iii) the structural features of the crystal phases, (iv) the local order of the glass structure<sup>8</sup> and diffusion properties derived from MD simulation, and, finally, (v) the morphology of the crystals determined by TEM observations.

The mechanism of growth of  $\text{Na}_2\text{CaSi}_2\text{O}_6$  in the  $x = 0$  glass occurs in two dimensions under diffusion control with an activation energy close to 200 kJ/mol. This behavior is derived from the following considerations:

(i) The crystallization process can be described by a mechanism consistent with an increase of  $n$  from 1 to 2 in the temperature range of 530–607 °C, as suggested by isothermal experiments, and then the value remains constant at 2 until 650 °C, as observed by nonisothermal ones.

(ii) The value of  $mE_a$  calculated with the nonisothermal method is  $406 \pm 10$  kJ/mol; by assuming  $m = 2$  (two-dimensional growth mechanism) a value of  $E_a$  ( $203 \pm 5$  kJ/mol) similar to that found by means of isothermal experiments ( $193 \pm 10$  kJ/mol) is obtained.

(iii) The  $\text{Na}_2\text{CaSi}_2\text{O}_6$  crystal structure is built up of stacked six-membered puckered silicate rings of formula  $[\text{Si}_6\text{O}_{18}]^{12-}$ ; the rings have a symmetrical form and are stacked in a ccp fashion along the  $c$ -axis direction.<sup>8</sup> The structure and cell parameters,  $a = b = 10.500$  Å and  $c = 13.184$  Å, suggest that the growth of this phase occurs with a two-dimensional mechanism (along the  $a$ - and  $b$ -axes).

(iv) The presence of six-membered rings is confirmed by the local structure of the  $x = 0$  glass obtained by MD classical simulation. In fact, the ring size distribution<sup>29</sup> shows that the most probable rings present in the  $x = 0$  glass structure are the  $[\text{Si}_6\text{O}_{18}]^{12-}$  ones. This suggests that the fundamental two-dimensional units that become ordered during the growth process are already present in the glass structure.

(v) To support this mechanism, the performed TEM analysis shows crystals characterized by a two-dimensional morphology (see Figure 9a).

These findings strongly suggest that the mechanism of growth occurs in two dimensions. Moreover, the  $n$  values reported in Table 5 claim a diffusion controlled crystallization mechanism with instantaneous nucleation rate at low temperature and constant nucleation rate at high temperature.

The kinetic analysis of  $\text{Na}_2\text{CaSi}_2\text{O}_6$  crystallization in the  $x = 0.68$  glass was performed at higher temperature with respect to that used for the  $x = 0$  glass in order to obtain results independent of the crystallization of  $\text{Na}_2\text{ZnSiO}_4$ .

Also, in this case the  $\text{Na}_2\text{CaSi}_2\text{O}_6$  crystallization process is controlled by diffusion with a two-dimensional growth. The rate-limiting step of the reaction is determined by the diffusion process of the glass cations. The activation energy of the crystallization is around 220 kJ/mol. These results are derived from the following considerations:

**TABLE 5: Avrami Exponent ( $n$ ) for the Crystallization Process<sup>30</sup>**

nucleation rate	phase boundary control model ( $n$ )	diffusion control model ( $n$ )
Three-Dimensional Growth ( $m = 3$ ) (Spherical Particles of Reactant)		
(1) constant	4	2.5
(2) zero (instantaneous)	3	1.5
(3) deceleratory	3–4	1.5–2.5
Two-Dimensional Growth ( $m = 2$ ) (Laminar Particles of Reactant)		
(1) constant	3	2
(2) zero (instantaneous)	2	1
(3) deceleratory	2–3	1–2
One-Dimensional Growth ( $m = 1$ ) (Lath-Shaped Particles of Reactant)		
(1) constant	2	1.5
(2) zero (instantaneous)	1	0.5
(3) deceleratory	1–2	0.5–1.5

(i) The isothermal method shows  $0.9 < n < 2.1$  in the temperature range 563–608 °C, in good agreement with the  $n$  value of  $\sim 2$  found with the nonisothermal method from 590 to 620 °C.

(ii) The value of  $mE_a$  calculated with the nonisothermal method is  $422 \pm 10$  kJ/mol; by assuming  $m = 2$  (two-dimensional growth mechanism), a value of  $E_a$  ( $211 \pm 5$  kJ/mol) similar to that found by means of isothermal experiments ( $223 \pm 10$  kJ/mol) is obtained.

(iii) The slightly higher value of  $E_a$  for the crystallization process of Na<sub>2</sub>CaSi<sub>2</sub>O<sub>6</sub> in the  $x = 0.68$  glass with respect to that found in  $x = 0$  glass (Table 6) can be explained by the increase of the activation energy of the diffusion process of the sodium ions in the Zn-containing glass (Table 5). The structural model obtained by MD shows that the number of six-membered rings ( $[\text{Si}_6\text{O}_{18}]^{12-}$ ) decreases dramatically compared to the  $x = 0$  glass because of the formation of polymeric long strings of  $[(\text{ZnO}_4)_m - (\text{SiO}_4)_N]_m$  tetrahedra with entrapped sodium ions.<sup>8</sup> The Na ions are found preferentially around the Zn tetrahedral units acting as charge compensators of the positive charge deficiency on the Zn tetrahedral units.<sup>31</sup> This strong electrostatic link prevents the diffusion process for Na ions; therefore higher energy for the Na diffusion process is required as determined by MD simulations (see Table 4). Similar behavior was detected in ref 32, where the activation energies of the static electrical conductivity of Na ions acting as a pure network modifier and as a charge compensator in SiO<sub>2</sub>–B<sub>2</sub>O<sub>3</sub>–Na<sub>2</sub>O glass were calculated.

The good agreement between the results obtained by isothermal and nonisothermal methods confirms the reliability of the nonisothermal method for the kinetics parameter calculations for silicate glasses.

The crystallization behavior of Na<sub>2</sub>ZnSiO<sub>4</sub> strictly resembles that of Na<sub>2</sub>CaSi<sub>2</sub>O<sub>6</sub> in  $x = 0.68$ . In fact, the growth can be ascribed to a two-dimensional process controlled by diffusion

of Na and Zn ions and the  $E_a$  for crystallization process is near 255 kJ/mol. This behavior is derived from the following considerations:

(i) Using the isothermal method  $n$  ranges from 0.9 to 2.2 (Table 6). At high temperature (590–620 °C), for the nonisothermal method,  $n$  is nearly constant (around 2), in good agreement with the value found with the isothermal method ( $n = 2.1$ ) (Table 6).

(ii) A mechanism controlled by diffusion with a two-dimensional growth ( $1 < n < 2$ ) is consistent with the crystal structure of Na<sub>2</sub>ZnSiO<sub>4</sub>, which is built up of two pyroxene-like chains along the  $c$ -axis: one chain is constituted by NaO<sub>4</sub> tetrahedra and the second one is constituted by alternate ZnO<sub>4</sub> and SiO<sub>4</sub> corner-shared tetrahedra. The first chain is considered cationic (Na) and the second anionic (Zn–Si).<sup>33</sup> The polar chains tend to join each other to form the two-dimensional layer (Table 5).

(iii) The speculation on the growth mechanism is also supported by the value of  $E_a$  found for the crystallization process. The comparison of the  $mE_a$  value ( $490 \pm 30$  kJ/mol) calculated from the nonisothermal method (from 590 to 620 °C) with the  $E_a$  value ( $266 \pm 15$  kJ/mol) calculated with the isothermal ones leads to  $m = 2$ .

(iv) The higher value of the  $E_a$  for the crystallization process of Na<sub>2</sub>ZnSiO<sub>4</sub> with respect to Na<sub>2</sub>CaSi<sub>2</sub>O<sub>6</sub> is well explained by the value of  $E_a$  for the diffusion process determined by MD simulations for zinc, calcium, and sodium ions (Table 4). In fact, there is a nearly linear correlation between the activation energy for the crystallization process (Table 6) and the sum of the activation energy of Na, Ca, and Zn ions (Table 6) made with respect to the crystal phases (i.e.,  $E_a$  of Na<sub>2</sub>CaSi<sub>2</sub>O<sub>6</sub> in  $x = 0$  glass vs  $E_a$  of Na in  $x = 0 + E_a$  of Ca in  $x = 0$  glass;  $E_a$  of Na<sub>2</sub>ZnSiO<sub>4</sub> in  $x = 0.68$  glass vs  $E_a$  of Na in  $x = 0.68 + E_a$  of Zn in  $x = 0.68$  glass). This confirms that the crystallization processes are controlled mainly by cation diffusion processes and there is a strong correlation between the energy values found for the crystallization and diffusion process. The value of  $D_0(\text{Zn})$  is surprisingly the highest compared to the ones for Ca<sup>2+</sup> and Na<sup>+</sup>. This can be due to the shorter mean Zn–Zn interatomic distance<sup>8</sup> with respect to the Ca–Ca and Na–Na ones, which implies a shorter jump for the Zn ion diffusion toward a vacant site occupied by the same ion type and, hence, a favored diffusion process is triggered by lowering the  $E_a$  for the diffusion. As a consequence, the temperature corresponding to the maximum of the exothermic peak of Na<sub>2</sub>ZnSiO<sub>4</sub> is lower with respect to Na<sub>2</sub>CaSi<sub>2</sub>O<sub>6</sub> ones.

(v) The morphological analysis performed by TEM confirms that the crystals of Na<sub>2</sub>ZnSiO<sub>4</sub> present a distinctive two-dimensional morphology (see Figure 9b).

## 5. Conclusions

The results obtained from crystallization kinetics show that the crystal phase Na<sub>2</sub>CaSi<sub>2</sub>O<sub>6</sub> is obtained from the

**TABLE 6: Comparison between the Avrami Exponent ( $n$ ), Apparent Activation Energy ( $E_a$ ), and Frequency Factor ( $A$ ) for the Different Systems**

glass	crystal phase	method <sup>a</sup>	Avrami exponent $n$	$E_a$ [kJ/mol]	$A$ [s <sup>-1</sup> ]
$x = 0$	Na <sub>2</sub> CaSi <sub>2</sub> O <sub>6</sub>	I	1.0 → 2.0 (530 → 607 °C)	193 ± 10	$1.2 \times 10^8$
		NI	2.1 → 2.4 (620 → 650 °C)	203 ± 5	
$x = 0.68$	Na <sub>2</sub> CaSi <sub>2</sub> O <sub>6</sub>	I	0.9 → 2.1 (563 → 608 °C)	223 ± 10	$1.6 \times 10^{10}$
		NI	2.1 → 2.3 (660 → 690 °C)	211 ± 5	
	Na <sub>2</sub> ZnSiO <sub>4</sub>	I	0.9 → 2.2 (563 → 608 °C)	266 ± 20	$3.1 \times 10^{12}$
		NI	2.1 → 2.2 (590 → 620 °C)	245 ± 15	

<sup>a</sup> I = isothermal method; NI = nonisothermal method.

$\text{Na}_2\text{O}\cdot\text{CaO}\cdot 2\text{SiO}_2$  ( $x = 0$ ) bioactive glass, and both  $\text{Na}_2\text{ZnSiO}_4$  and  $\text{Na}_2\text{CaSi}_2\text{O}_6$  are obtained from  $0.68\text{ZnO}\cdot\text{Na}_2\text{O}\cdot\text{CaO}\cdot 2\text{SiO}_2$  ( $x = 0.68$ ).

The  $\text{Na}_2\text{CaSi}_2\text{O}_6$  and  $\text{Na}_2\text{ZnSiO}_4$  crystallizations occur by a bidimensional diffusion controlled mechanism and show independence from temperature. Zinc addition to the bioactive glass produces an increment of the crystallization temperature of  $\text{Na}_2\text{CaSi}_2\text{O}_6$ .

A rationalization of the behavior observed experimentally is offered by the results of computational simulation studies which provide insight into the glass structure.

A significant reduction of the polymerization of silica network is observed in the zinc-containing glass caused by the disruption of six-membered rings ( $[\text{Si}_6\text{O}_{18}]^{12-}$ ) characteristic of the  $\text{Na}_2\text{O}\cdot\text{CaO}\cdot 2\text{SiO}_2$  glass and the formation of strings formed by  $[(\text{ZnO}_4)_n-(\text{SiO}_4)_N]_m$  units. The decrement of strength of network, also detected by a decrement of  $T_g$  determined in ref 8, might be responsible for the increase of the  $\text{Na}_2\text{CaSi}_2\text{O}_6$  rate constants.

Moreover, the prevailing charge compensator role of the Na ions with respect to the charge deficiency on the Zn tetrahedral units can be invoked to explain the increment of  $E_a$  for the crystallization process of  $\text{Na}_2\text{CaSi}_2\text{O}_6$  in the zinc-containing glass, as also confirmed by the results of a leaching test performed on glass with a similar composition where the sodium ions release decreases as a function of Zn content.<sup>8,9</sup>

**Acknowledgment.** This work was supported by Ministero dell'Università e della Ricerca Scientifica e Tecnologica (MIUR, Grant 2006032335\_004). The authors are grateful to the technicians of the CIGS (Centro Interdipartimentale Grandi Strumenti, The University of Modena and Reggio Emilia) for their help with XRD and TEM analyses.

## References and Notes

- (1) Hench, L. L.; Polak, J. M. *Science* **2002**, *295*, 1014.
- (2) Hench, L. L.; Splinter, R. J.; Allen, W. C.; Greenlee, T. K. *J. Biomed. Mater. Res. Symp.* **1971**, *2*, 117.
- (3) Philo, O. P.; LaTorre, G. P.; Hench, L. L. *J. Biomed. Mater. Res.* **1996**, *30*, 509.
- (4) Xynos, I. D.; Edgar, A. J.; Buttery, L. D. K.; Hench, L. L.; Polak, J. M. *J. Biomed. Mater. Res.* **2001**, *55*, 141.

- (5) Ito, A.; Kawamura, H.; Otsuka, M.; Ikeuchi, M.; Ohgushi, H.; Ishikawa, K.; Onuma, K.; Kanzaki, N.; Sogo, Y.; Ichinose, N. *Mater. Sci. Eng., C* **2002**, *22*, 21.
- (6) Du, R. L.; Chang, J.; Ni, S. Y.; Zhai, W. Y.; Wang, J. Y. *J. Biomater. Appl.* **2006**, *20*, 341.
- (7) Avrami, M. *J. Chem. Phys.* **1941**, *9*, 177.
- (8) Lusvardi, G.; Malavasi, G.; Menabue, L.; Menziani, M. C. *J. Phys. Chem. B* **2002**, *106*, 9753.
- (9) Linati, L.; Lusvardi, G.; Malavasi, G.; Menabue, L.; Menziani, M. C.; Mustarelli, P.; Segre, U. *J. Phys. Chem. B* **2005**, *109*, 4989.
- (10) Kim, H. M.; Miyaji, F.; Kokubo, T.; Ohtsuki, C.; Nakamura, T. *J. Am. Ceram. Soc.* **1995**, *78*, 2405.
- (11) Marotta, A.; Saiello, S.; Branda, A.; Buri, A. *J. Mater. Sci.* **1982**, *17*, 105.
- (12) Mazzuccato, E.; Artioli, G.; Gualtieri, A. *Phys. Chem. Miner.* **1999**, *26*, 375.
- (13) Ruitenberg, G.; Woldt, E.; Petford-Long, A. K. *Thermochim. Acta* **2001**, *378*, 97.
- (14) Avrami, M. *J. Chem. Phys.* **1939**, *7*, 1103.
- (15) Hench, J. D.; Sharp, H. J. *J. Am. Ceram. Soc.* **1972**, *55*, 74.
- (16) Bamford, C. H.; Tipper, C. F. H. In *Comprehensive chemical kinetics*; Elsevier: New York, 1980; pp 22, 41–49.
- (17) Ozawa, T. *Polymer* **1971**, *12*, 150.
- (18) Matusita, K.; Sakka, S. *J. Non-Cryst. Solids* **1980**, *38&39*, 741.
- (19) Kissinger, H. E. *J. Res. Natl. Bur. Stand.* **1956**, *57*, 217.
- (20) Matusita, K.; Konatsu, T.; Yokota, R. *J. Mater. Sci.* **1984**, *19*, 291.
- (21) Clupper, D. C.; Hench, L. L. *J. Non-Cryst. Solids* **2003**, *318*, 43.
- (22) Gotor, F. J.; Criado, J. M.; Malek, J. *J. Am. Ceram. Soc.* **2001**, *84*, 1797.
- (23) Smith, W.; Forester, T. R. *J. Mol. Graphics* **1996**, *14*, 136.
- (24) Pedone, A.; Malavasi, G.; Menziani, M. C.; Cormack, A. N.; Segre, U. *J. Phys. Chem. B* **2006**, *110*, 11780.
- (25) Cormack, A. N.; Du, J.; Zeitler, T. R. *Phys. Chem. Chem. Phys.* **2002**, *4*, 3193.
- (26) Allen, M. P.; Tildesley, D. J. *Computer Simulation of Liquids*; Clarendon Press: Oxford, 1989.
- (27) Cheng, K. *J. Mater. Sci.* **2001**, *36*, 1043 and references therein.
- (28) Ferrari, A. M.; Leonelli, C.; Pellacani, G. C.; Siligardi, C. *J. Non-Cryst. Solids* **2003**, *315*, 77.
- (29) Lusvardi, G.; Malavasi, G.; Menabue, L.; Menziani, M. C.; Segre, U.; Carnasciali, M. M.; Ubaldini, A. *J. Non-Cryst. Solids* **2004**, *345&346*, 710.
- (30) Hulbert, S. F. *J. Br. Ceram. Soc.* **1969**, *6*, 11.
- (31) Delaye, J. M.; Cormier, L.; Ghaleb, D.; Calas, G. *J. Non-Cryst. Solids* **2001**, *290*, 293–295.
- (32) Grandjean, A.; Malki, M.; Simonnet, C. *J. Non-Cryst. Solids* **2006**, *352*, 2736.
- (33) Plakhov, G. F.; Belov, N. V. *Sov. Phys. Crystallogr.* **1979**, *24* (6), 674.